EFFECT OF FIBER STRENGTH AND FIBER-MATRIX INTERFACE ON CRACK BRIDGING IN CEMENT COMPOSITES

By Tetsushi Kanda[1] and Victor C. Li,[2] Member, ASCE

ABSTRACT: This article proposes a new theory for predicting the crack-bridging performance of random short fibers involved in cementitious composites. The current theoretical model for estimating crack bridging performance of random short fiber reinforced cement composites under tension is limited to specific constituent properties: friction-dominant fiber-matrix interface and complete fiber pull-out from matrix without rupture. The new theory extends this model by accounting for two often-encountered features in practice: fiber strength reduction and rupture in composites, and chemical bond–dominant fiber-matrix interface. The new theory was verified to capture important characteristics in bridging performance in comparison with composite tensile test data. As a result, the new theory forms an important foundation for developing high-performance random short fiber reinforced cement composites.

INTRODUCTION

Crack bridging by fiber has been recognized as one of the most important fundamental properties governing composite response. The mechanism of crack bridging has been substantially investigated in the areas of fiber-reinforced plastic (e.g., Outwater and Murphy 1970; Takaku and Arridge 1973), metal (e.g., Kelly and Tyson 1965), ceramics (e.g., Marshall and Cox 1988), and cement (e.g., Shao et al. 1993). Furthermore, crack bridging has been recognized to even control structural response (e.g., Horii and Nanakorn 1993; Naaman and Reinhardt 1995; Stang et al. 1995).

For purposes of composite material engineering and structural performance design based on composite microstructure control, it is desirable to relate the crack-bridging stress versus crack-opening relation (σ-δ) to fiber, matrix, and interface properties. This relation is known as ''bridging law'' and has been extensively investigated, especially in the area of fiber-reinforced ceramics (Marshall et al. 1985; Gao et al. 1988; Hutchinson and Jensen 1990; Bao and Song 1993). However, these investigations are for composites reinforced with unidirectionally aligned fiber, and bridging law with randomly aligned short fiber has been little clarified (Bao and Suo 1992). This has been recently accomplished by Li and Leung (1992) and Li (1993) but for the special case where flexible fiber pull-out and friction-dominated interface are assumed. The resulting σ-δ relation has been successfully deployed for the design of very ductile cementitious composites (Li 1993).

To broaden the range of fibers useful to design random short fiber reinforced cement composites (RSFRCC), it is desirable to extend the current theory to handle composites containing fibers which may break during crack opening in the bridging process. In addition, some fibers such as polyvinyl alcohol (PVA) have very high chemical bonding in cementitious composites. While PVA fiber has been recognized as high potential reinforcement in cementitious composites due to its high strength, this potential has not yet been fully realized (Akihama et al. 1985; Betterman 1995).

The present paper extends the work of Li and coworkers (Li and Leung 1992; Li 1993; Maalej et al. 1995) by developing a new theory grounded on experimentally observed interface and crack-bridging behavior of PVA fiber. Although the parametric values used for model validation are based on this specific fiber, the model itself can be applied to various flexible polymeric fiber types having the following characteristics: (1) The fiber-matrix interface debonding is governed by chemical bond in addition to frictional sliding after debonding; (2) a crack-bridging fiber may rupture during crack-opening process when its tensile strength is exceeded; and (3) the fiber tensile strength may be reduced due to inclined-angle bridging. The first two characteristics may be found in a variety of fibers, while the third may be unique to some polymeric fibers. All three characteristics have been documented in detail for PVA fibers (Kanda and Li 1998a).

In the following, the crack-bridging stress–displacement relation for a single fiber pulled out with normal and inclined angle is first derived accounting for chemical bond and fiber strength reduction due to inclined angle. This single-fiber stress-displacement relation is then implemented into a composite model that treats fiber orientation and centroidal location as statistically random. The resulting crack-bridging stress–crack-opening displacement relationship is then verified using uniaxial tensile test data of a PVA fiber composite. Finally, parametric study of this composite model reveals that the newly introduced features strongly affect the crack-bridging performance of composites.

The ultimate purpose of this study is to achieve the design of very ductile fiber-reinforced cement-based composites, which show tensile strain capacity attaining several percent and are called pseudo strain hardening (PSH) composites, by using high-performance hydrophilic PVA fiber or fibers of similar type. The present study lays the foundation for this ultimate goal. This subject is taken up in a companion paper (Kanda and Li 1998c, in press). As well, better understanding is achieved for the tensile response of these composites.

CRACK-BRIDGING STRESS–DISPLACEMENT RELATION

Single-Fiber Stress–Displacement Relationship for Chemical-Type Interface

Fiber-matrix interfacial shear resistance is generally classified into two categories, i.e., friction-dominant type and chemical bond–dominant type (Kanda and Li 1998a). The former's behavior is governed by a frictional shear stress τ_i; the latter type can be described by a chemical bond strength τ_s in addition to τ_i (e.g., Goplaratnam and Shah 1985).

For a single fiber with friction type interface embedded in a matrix, the single-fiber bridging stress, $\sigma_{d|\text{friction}'}$ is related to the crack opening displacement (COD) δ, assumed to be twice

[1]Sr. Res. Engr., Kajima Tech. Res. Inst., 2-19-1 Tobitakyu, Chofu-shi, Tokyo 182, Japan.

[2]Prof. and Dir., ACE-MRL, Dept. of Civ. and Envir. Engrg., Univ. of Michigan, Ann Arbor, MI 48109-2125.

Note. Associate Editor: Gilles Pijaudier-Cabot. Discussion open until August 1, 1999. To extend the closing date one month, a written request must be filed with the ASCE Manager of Journals. The manuscript for this paper was submitted for review and possible publication on September 6, 1996. This paper is part of the ***Journal of Engineering Mechanics***, Vol. 125, No. 3, March, 1999. ©ASCE, ISSN 0733-9399/99/0003-0290–0299/$8.00 + $.50 per page. Paper No. 14038.

the fiber displacement at crack plane. This is achieved as a result of ''shear-lag analysis'' (Li and Leung 1992), as in the following formula [an identical expression was derived via stress-intensity analysis (Marshall et al. 1985)]:

$$\sigma_d|_{\text{friction}} = \left[4(1+\eta)\tau_i E_f \left(\frac{\delta}{d_f}\right)\right]^{1/2} = \lambda \left(\frac{\hat{\delta}}{\hat{\delta}_i^*}\right)^{1/2}$$

$$\text{for } \delta \le \delta_{0i} (\hat{\delta} \le \hat{\delta}_{0i}) \tag{1}$$

where $\eta = V_f E_f/[(1 - V_f)E_m]$; $\sigma_{0i} = V_f\lambda/4$; $\hat{\delta} = 2\delta/L_f$; $\hat{\delta}_i^* = \lambda/[E_f(1+\eta)]$; $\lambda = 2\tau_i(L_f/d_f)$; and $\hat{\delta}_{0i} = \hat{\delta}_i^* \hat{l}^2$. V_f = fiber volume fraction; L_f = fiber length; l = fiber embedment length; τ_i = frictional bond strength; E_f = elastic modulus of fiber; d_f = fiber diameter; and E_m = elastic modulus of matrix. [Note: All quantities of (ˆ) have been normarized by the half-fiber length $L_f/2$.] Eq. (1) is valid for small $\delta < \delta_{oi}$ when debonding terminates and fiber end slip commences (debonding stage). In this model, chemical bond is neglected and the shear stress distribution is represented only by constant friction τ_i, as shown in Fig. 1(a). Furthermore, after fiber end slip initiates (pull-out stage), the bridging stress $\sigma_p|_{\text{friction}}$ during pull-out decays with COD δ (Li and Leung 1992)

$$\sigma_p|_{\text{friction}} = \frac{4\tau_i}{d_f}(l + \delta_{0i} - \delta) = \lambda(\hat{l} + \hat{\delta}_{0i} - \hat{\delta})$$

$$\text{for } \delta_{0i} < \delta \le l (\hat{\delta}_{0i} < \hat{\delta} \le \hat{l}) \tag{2}$$

For the interface with both chemical and friction bonds, shear stress distribution along a fiber is illustrated as in Fig. 1(b). Then, the stress-COD relationships (1) and (2) should be modified according to the shear stress distribution. Fiber stress in the debonding stage, σ_d, and that in the pull-out stage, σ_p, are represented as follows (Appendices I and II):

$$\sigma_d = \lambda \left[\left(\frac{\hat{\delta}}{\hat{\delta}_i^*}\right) + \beta^2\right]^{1/2} \tag{3}$$

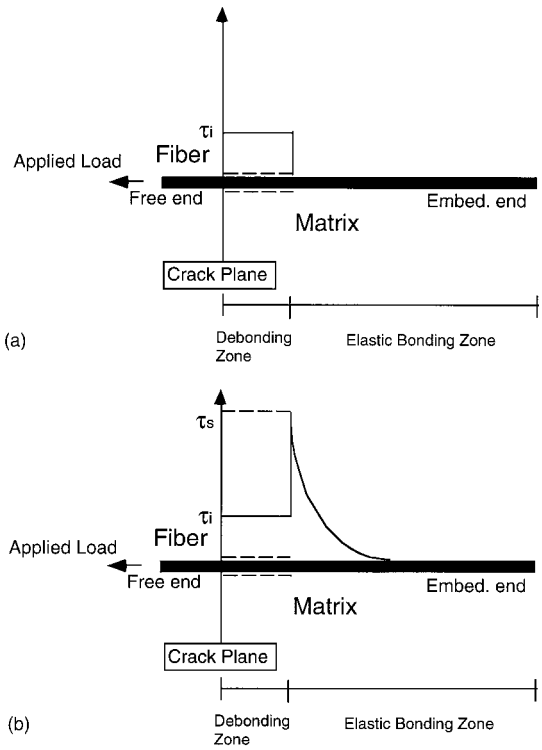

FIG. 1. Assumption of Shear Stress Distribution: (a) in Original Friction-Only Interface Model; (b) in Chemical Bond and Friction Interface Model

$$\sigma_p = \lambda\,[\{1 + 2\beta\hat{\delta}_i^*\}\hat{l} + \hat{\delta}_{0i} - \hat{\delta}] \tag{4}$$

where $\beta = \sigma_{ds}/\lambda$. σ_{ds} denotes portion of fiber stress sustained by chemical bond τ_s, and is defined in (27). It is noted that (3) and (4) reduce to (1) and (2) when $\sigma_{ds} = 0$, corresponding to no chemical bond interface.

Eqs. (3) and (4) were derived for the case of straight short fiber that is aligned with the loading direction and is also perpendicular to the propagating crack surface in fiber-reinforced composites. In the more general case of RSFRCC, fibers will intersect the propagating crack at different angles. An obliquely oriented flexible fiber can lead to a higher bridging force across a matrix crack plane than that of a straightly aligned fiber, for the same crack opening. This load increase becomes more significant with inclining angle ϕ between the fiber and loading axis, and is representable by a snubbing coefficient f (Li et al. 1990). The general form of single-fiber bridging stress was expressed by (Maalej et al. 1995)

$$\sigma_b = \begin{cases} \sigma_b(\hat{\delta}, \phi) = \sigma_d e^{f\phi} & \text{for } \delta \le \delta_0 (\hat{\delta} \le \hat{\delta}_0) \\ \sigma_b(\hat{\delta}, \phi, \hat{l}) = \sigma_p e^{f\phi} & \text{for } \delta > \delta_0 (\hat{\delta} > \hat{\delta}_0) \end{cases} \tag{5}$$

where $\hat{\delta}_0 = \hat{\delta}_i^*[\hat{l}^2 + 2\beta\hat{l}]$. δ_0 denotes COD δ at peak fiber stress during the debonding stage, whose derivation is shown in Appendix II.

Apparent Fiber Strength in Composites

Fiber rupture in composites reinforced with unidirectional continuous fiber has been examined in many research studies (Kelly and Tyson 1965; Marshall and Cox 1987; Hutchinson and Jensen 1990). However, fiber rupture for RSFRCCs was fully clarified neither experimentally nor theoretically. This phenomenon was quite recently investigated using short fibers obliquely embedded in cementitious matrices (Kanda and Li 1998a).

It has been reported that the apparent strength of high-strength hydrophilic PVA fibers embedded in a cementitious composite tends to be less than the strength reported by manufacturers that is typically obtained from standard tests like ASTM D 2101-94 (Kanda and Li 1998a). This strength degradation effect was investigated through pull-to-rupture tests, in which one end of a single fiber is embedded in a matrix foundation and the other end is pulled to rupture the fiber. These tests revealed that the strength degradation phenomenon is probably associated with (1) fiber surface abrasion; (2) spalling of the matrix foundation; and (3) fiber bending, all of which are intensified with fiber's inclining angle ϕ. Therefore, this effect can be phenomenologically represented as a function of angle ϕ as follows (Kanda and Li 1998a):

$$\sigma_{fu} = \sigma_{fu}^n e^{-f'\phi} \tag{6}$$

where σ_{fu} = apparent fiber strength; σ_{fu}^n = nominal tensile strength of fiber; and f' = apparent fiber strength reduction factor ($f' > 0$). Note that σ_{fu} is experimentally obtained by dividing the apparently sustained load by the sectional area of a fiber obliquely embedded into matrix, and that σ_{fu}^n denotes the strength of an embedded fiber with $\phi = 0$, which is lower than the one obtained by the standard fiber strength tests. Furthermore, f' is determined by the curve fitting of test results obtained from specimens with different ϕ. For a PVA fiber, $f' = 0.3$ and $\sigma_{fu}^n = 1{,}666$ MPa were obtained experimentally (Kanda and Li 1998a).

Effect of Fiber Rupture on Single-Fiber Bridging Stress

Apparent fiber strength as well as chemical bond should be taken into account in a single-fiber bridging model for high-

strength hydrophilic fiber composites. These two aspects promote fiber rupture and influence the mechanical behavior of the composites. The current study proposes a new bridging law for the composites that extends the original fiber rupture pull-out model, FRPM (Maalej et al. 1995), to cover the above observed phenomena by introducing two additional micromechanical parameters, chemical bond strength τ_s and apparent fiber-strength reduction factor f'.

Originally intact fiber population at the opening crack plane in composites decreases with increasing COD δ or fiber bridging stress σ_b due to fiber rupture. This phenomenon should be mathematically represented to establish the new bridging law. Understanding the phenomenon is facilitated by employing fiber-rupture spaces (FRS) with two dimensions, angle ϕ and embedment length l. FRS represents the condition of fiber rupture and the population of ruptured fiber in terms of (l, ϕ) combination. Two kinds of FRS are considered, i.e., potential FRS, S_p, and current FRS, S_c. The boundaries of these two FRSs are determined by micromechanics parameters of composite systems. The first FRS, S_p, is illustrated in Fig. 2, where fibers with (l, ϕ) combinations inside the S_p space are expected to fail by rupture or remain bridging a crack without being pulled out. The boundary between S_p and the intact fiber space is defined as the critical length l_u, the minimum embedment length leading to fiber rupture. The l_u decreases with increase of inclining angle ϕ since fiber bridging stress σ_b increases with ϕ due to the snubbing effect. Therefore, higher ϕ results in increasing possibility of fiber rupture. The l_u is derived by equating σ_d at rupture to maximum single fiber bridging stress σ_{max} (at completion of debonding) defined by (29). The σ_d at rupture is obtained by setting bridging stress σ_b in (5) equal to fiber strength σ_{fu} in (6)

$$\hat{l}_u(\phi) = \hat{L}_{ci}[e^{-(f+f')\phi} - \xi] \tag{7}$$

where $\hat{L}_{ci} = (\sigma_{fu}^n/\lambda)$ and $\xi = \sigma_{ds}/\sigma_{fu}^n$. The $\hat{l}_u$ becomes identical to the one defined in the original FRPM when $f' = \xi = 0$ as shown in Fig. 2. Furthermore, Fig. 2 shows that l_u is significantly reduced by the effects of f' and ξ compared with the original one, thereby resulting in a much larger rupture space. The l_u attains the minimum value ($L_r/2$) at $\phi = \pi/2$ and the maximum (L_c) at $\phi = 0$. These extremes are defined using (7):

$$\frac{\hat{L}_r}{2} = \hat{L}_{ci}[e^{-(f+f')\pi/2} - \xi] \tag{8}$$

$$\hat{L}_c = \hat{L}_{ci}(1 - \xi) \tag{9}$$

For a given fiber with maximum embedment length of $L_f/2$, there exists the minimum angle below which fiber rupture never occurs. This angle is defined as the potential fiber-rupture angle ϕ_b (Fig. 2), so that only fibers lying at an inclination angle higher than ϕ_b have the potential to rupture. ϕ_b is obtained by setting l_u in (7) equal to $L_f/2$

$$\phi_b = \begin{cases} \dfrac{\pi}{2} & \text{for } L_f < L_r \\ -\dfrac{1}{f+f'} \ln\left(\dfrac{1}{\hat{L}_{ci}} + \xi\right) & \text{for } L_r < L_f < 2L_c \\ 0 & \text{for } 2L_c < L_f \end{cases} \tag{10}$$

Finally, the potential fiber-rupture space S_p (shaded region, Fig. 2) can be expressed as

$$S_p = \left\{ l \in \left[\frac{L_r}{2}, \frac{L_f}{2}\right], \phi \in \left[\phi_b, \frac{\pi}{2}\right] \middle\| \; l \geq l_u \right\} \tag{11}$$

The second rupture space, S_c, represents the degree of fiber rupture at any COD δ during crack opening, and is depicted in Fig. 3. The S_c starts from empty and expands with increase of δ so as to eventually coincide with the potential rupture space S_p. This conveys that fibers having large embedment length, and oriented at a high angle to the loading axis, fail first as the composite crack opens. The S_c is bounded by inclining angle ϕ_c, below which no fiber rupture occurs at certain δ. ϕ_c is named current rupture angle and expressed as follows (Appendix III):

$$\phi_c(\hat{\delta}) = \begin{cases} \dfrac{\pi}{2} & \text{for } \delta < \delta_u \left(\phi = \dfrac{\pi}{2}\right) \\ -\dfrac{1}{2(f+f')} \ln\left[\left(\dfrac{\hat{\delta}}{\hat{\delta}_i^*}\right)\dfrac{1}{\hat{L}_{ci}^2} + \xi^2\right] & \text{for } \delta_u \left(\phi = \dfrac{\pi}{2}\right) \leq \delta \leq \delta_{ue} \\ \phi_b & \text{for } \delta_{ue} < \delta \end{cases} \tag{12}$$

$\delta_u(\phi = \pi/2)$ corresponds to minimum COD at which fibers oriented at $\phi = \pi/2$ first rupture, while δ_{ue} denotes COD when debonding stage is completed (see Appendix III). The S_c is then expressed with a formula similar to S_p

$$S_c = \left\{ l \in \left[\frac{L_r}{2}, \frac{L_f}{2}\right], \phi \in \left[\phi_c, \frac{\pi}{2}\right] \middle\| \; l \geq l_u \right\} \tag{13}$$

Besides the ruptured fibers, those completely pulled out of a matrix at a given δ should be distinguished, since they no longer contribute to bridging crack planes. For these fibers, complete fiber pull-out space S_e is introduced. After debonding is completed, surviving fibers are limited in embedment length to less than l_u since, due to rupture, fibers with $l > l_u$ are no longer intact. Thereafter, all the intact fibers with ϕ are com-

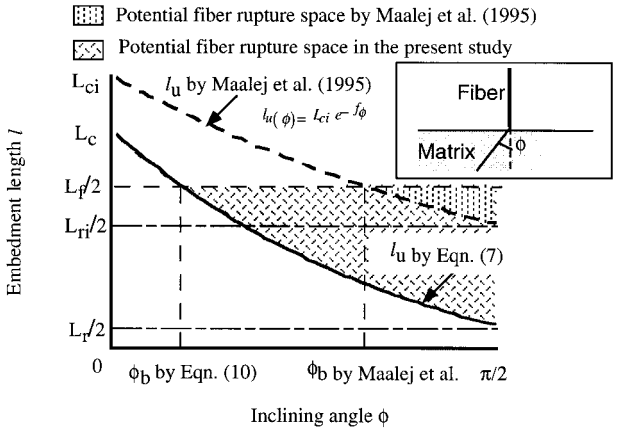

FIG. 2. Potential Fiber-Rupture Space S_p

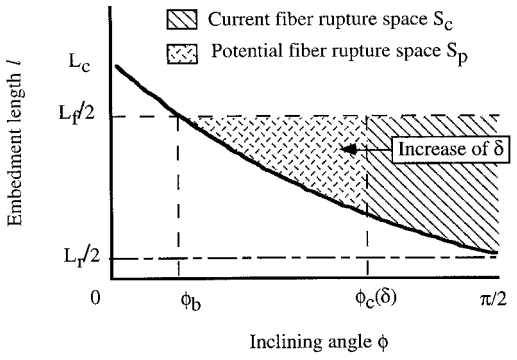

FIG. 3. Current Fiber-Rupture Space S_c

pletely pulled out of a matrix when δ reaches $l_u(\phi)$. This angle ϕ_a is derived by setting l_u in (7) to δ

For $L_r \le L_f \le 2L_c$:

$$\phi_a(\hat{\delta}) = \begin{cases} \dfrac{\pi}{2} & \text{for } \delta \le \dfrac{L_r}{2} \\ -\dfrac{1}{(f+f')} \ln\left[\dfrac{\hat{\delta}}{\hat{L}_{ci}} + \xi\right] & \text{for } \dfrac{L_r}{2} < \delta < \dfrac{L_f}{2} \\ \phi_b & \text{for } \delta = \dfrac{L_f}{2} \end{cases} \tag{14a}$$

For $2L_c < L_f$:

$$\phi_a(\hat{\delta}) = \begin{cases} \dfrac{\pi}{2} & \text{for } \delta \le \dfrac{L_r}{2} \\ -\dfrac{1}{(f+f')} \ln\left[\dfrac{\hat{\delta}}{\hat{L}_{ci}} + \xi\right] & \text{for } \dfrac{L_r}{2} < \delta < L_c \\ \phi_b & \text{for } \delta = L_c \end{cases} \tag{14b}$$

Similar to ϕ_c in (12), ϕ_a starts from $\pi/2$ and eventually reaches ϕ_b defined by (10) as δ increases. The above formulas show that fiber bridging is terminated at $\delta = L_f/2$ for $L_r < L_f < 2L_c$ or at $\delta = L_c$ for $2L_c < L_f$. The complete pull-out space S_e is then expressed

$$S_e = \left\{ l \in \left[0, \frac{L_f}{2}\right], \phi \in [0, \phi_b] \middle\| 0 \le l \le \delta \right\} \cup \left\{ l \in \left[0, \frac{L_f}{2}\right], \phi \in \left[\phi_b, \frac{\pi}{2}\right] \middle\| \phi_a \le \phi \le \frac{\pi}{2} \right\} \tag{15}$$

Based on the preceding discussion, the single-fiber bridging model expressed by (5) is finally modified as follows:

$$\sigma_b(\hat{\delta}, \phi, \hat{l}) = \begin{cases} \begin{cases} \sigma_d e^{f\phi} & \text{for } (\delta, \phi, l) \notin S_c \\ 0 & \text{for } (\delta, \phi, l) \in S_c \end{cases} & \text{for } \delta \le \delta_0 \\ \begin{cases} \sigma_p e^{f\phi} & \text{for } (\delta, \phi, l) \notin S_e \\ 0 & \text{for } (\delta, \phi, l) \in S_e \end{cases} & \text{for } \delta > \delta_0 \end{cases} \tag{16}$$

It should be noted that nominal fiber strength is assumed deterministic in this study whereas the rupture strength of polymeric fiber is better being treated statistically. However, no test data are currently available to determine variability of nominal fiber strength, and the variability investigation is beyond the scope of this article. Such investigation and the subsequent statistical fiber strength treatment for crack-bridging theory should be undertaken in future studies.

Composite Bridging Stress-COD Relation

A bridging law has been developed for RSFRCCs by introducing the stochastic approach by Li and Leung (1992). They derived composite bridging stress σ_c-δ relation for the short fiber composites, which (assuming the composites involve no fiber rupture) was expressed by the following formula (Maalej et al. 1995):

$$\sigma_c = \frac{V_f}{2} \int_0^{\pi/2} \int_0^1 \sigma_b(\hat{\delta}, \phi, \hat{l}) \sin 2\phi \, d\hat{l} \, d\phi \tag{17}$$

To account for fiber rupture and chemical bond, (17) is modified as (18) and (19) by employing (16)

$$\sigma_c = \frac{V_f}{2} \left\{ \int_0^{\phi_c} \int_{\hat{l}_0}^1 \sigma_d e^{f\phi} \sin 2\phi \, d\hat{l} \, d\phi + \int_0^{\phi_c} \int_{\hat{\delta}}^{\hat{l}_0} \sigma_p e^{f\phi} \sin 2\phi \, d\hat{l} \, d\phi + \int_{\phi_c}^{\pi/2} \int_{\hat{\delta}}^{\hat{l}_u} \sigma_p e^{f\phi} \sin 2\phi \, d\hat{l} \, d\phi \right\} \quad \text{for } 0 \le \delta < \delta_{ue} \tag{18}$$

$$\sigma_c = \frac{V_f}{2} \left\{ \int_0^{\phi_b} \int_{\hat{\delta}}^1 \sigma_p e^{f\phi} \sin 2\phi \, d\hat{l} \, d\phi + \int_{\phi_b}^{\phi_a} \int_{\hat{\delta}}^{\hat{l}_u} \sigma_p e^{f\phi} \sin 2\phi \, d\hat{l} \, d\phi \right\} \quad \text{for } \delta_{ue} \le \delta \le \min\left(\frac{L_f}{2}, L_c\right) \tag{19}$$

where $\hat{l}_0 = -\beta + [(\hat{\delta}/\hat{\delta}_i^*) + \beta^2]^{1/2}$. The $\delta < \delta_0$ in (16) correponds to $\hat{l} > \hat{l}_0$ in (18) and (19). The σ_c-δ relation represented by (18) is defined as the debonding stage, and that by (19) is called the pull-out stage. These stages are demarcated by δ_{ue}, where the debonding process of all fibers is terminated (expression of δ_{ue} is described in Appendix III). By evaluating integrals in the above formulas, the σ_c-δ relation is derived as (see Appendix IV for detail)

For $L_r < L_f < 2L_c$:

$$\sigma_c = \begin{cases} \sigma_{0i} d C_A G\left(\dfrac{\pi}{2}, f\right) & \text{for } 0 \le \delta \le \delta_u\left(\phi = \dfrac{\pi}{2}\right) \\ \sigma_{0i} \left\{ \begin{matrix} dC_A G(\phi_c, f) + {}_dC_{B2} A(\phi_c, -f-2f') \\ + {}_dC_{B3} A(\phi_c, -f') + {}_dC_{B4} A(\phi_c, f) \end{matrix} \right\} & \text{for } \delta_u\left(\phi = \dfrac{\pi}{2}\right) < \delta \le \delta^* \\ \sigma_{0i} \left\{ \begin{matrix} {}_pC_C G(\phi_b, f) + {}_pC_{B2} A(\phi_b, -f-2f') \\ + {}_pC_{B3} A(\phi_b, -f') + {}_pC_{B4} A(\phi_b, f) \end{matrix} \right\} & \text{for } \delta^* < \delta \le \dfrac{L_r}{2} \\ \sigma_{0i} \left\{ \begin{matrix} {}_pC_C G(\phi_b, f) + {}_pC_{B2} B(\phi_b, \phi_a, -f-2f') \\ + {}_pC_{B3} B(\phi_b, \phi_a, -f') + {}_pC_{B4} B(\phi_b, \phi_a, f) \end{matrix} \right\} & \text{for } \dfrac{L_r}{2} < \delta \le \dfrac{L_f}{2} \end{cases} \tag{20}$$

For $L_f > 2L_c$:

$$\sigma_c = \begin{cases} \sigma_{0i} d C_A G\left(\dfrac{\pi}{2}, f\right) & \text{for } 0 \le \delta \le \delta_u\left(\phi = \dfrac{\pi}{2}\right) \\ \sigma_{0i} \left\{ \begin{matrix} {}_dC_A G(\phi_c, f) + {}_dC_{B2} A(\phi_c, -f-2f') \\ + {}_dC_{B3} A(\phi_c, -f') + {}_dC_{B4} A(\phi_c, f) \end{matrix} \right\} & \text{for } \delta_u\left(\phi = \dfrac{\pi}{2}\right) < \delta \le \delta_c \\ \sigma_{0i} \left\{ {}_pC_{B2} G\left(\dfrac{\pi}{2}, -f-2f'\right) + {}_pC_{B3} G\left(\dfrac{\pi}{2}, -f'\right) + {}_pC_{B4} G\left(\dfrac{\pi}{2}, f\right) \right\} & \text{for } \delta_c < \delta \le \dfrac{L_r}{2} \\ \sigma_{0i} \{ {}_pC_{B2} G(\phi_a, -f-2f') + {}_pC_{B3} G(\phi_a, -f') + {}_pC_{B4} G(\phi_a, f) \} & \text{for } \dfrac{L_r}{2} < \delta \le \dfrac{L_f}{2} \end{cases} \tag{21}$$

where

$$\gamma = \left(\frac{\hat{\delta}}{\hat{\delta}_i^*}\right) + \beta^2$$

$${}_dC_A = -\gamma + 2\gamma^{1/2} + \beta^2,\ {}_dC_{B2} = \hat{L}_{ci}^2,\ {}_dC_{B3} = -2\hat{L}_{ci}^2\xi,\ {}_dC_{B4} = \hat{L}_{ci}^2\xi^2,$$

$${}_dC_C = 1$$

$${}_pC_A = -\gamma + 2\gamma^{1/2} + \beta^2 - 2\hat{\delta}\gamma^{1/2} + 2\hat{\delta}\beta + \hat{\delta}^2$$

$${}_pC_{B2} = \hat{L}_{ci}^2,\ {}_pC_{B3} = -2\hat{L}_{ci}^2\xi - 2\hat{\delta}\hat{L}_{ci}$$

$${}_pC_{B4} = \hat{L}_{ci}^2\xi^2 + 2\hat{\delta}\hat{L}_{ci}\xi + \hat{\delta}^2,\ {}_pC_C = 1 - 2\hat{\delta} + \hat{\delta}^2$$

$$G(\phi, \alpha) = \frac{1}{\alpha^2 + 4}\{e^{\alpha\phi}[\alpha \sin 2\phi - 2\cos 2\phi] + 2\}$$

$$A(\phi, \alpha) = \frac{1}{\alpha^2 + 4}\{e^{\alpha\phi}[2\cos 2\phi - \alpha \sin 2\phi] + 2e^{\pi\alpha/2}\}$$

$$B(\phi_1, \phi_2, \alpha) = \frac{1}{\alpha^2 + 4}\{e^{\alpha\phi_2}[\alpha \sin 2\phi_2 - 2\cos 2\phi_2] + e^{\alpha\phi_1}[2\cos 2\phi_1 - \alpha \sin 2\phi_1]\}$$

Eqs. (20) and (21) show that the proposed bridging law consists of several micromechanical parameters such as γ, β, and ξ. Considering the expressions for these parameters described earlier, this bridging law can be represented in a normalized form by employing normalized bridging stress $\bar{\sigma}_c$ and normalized COD $\hat{\delta}$, as follows:

$$\bar{\sigma}_c = \text{func}\left(\frac{E_f}{\lambda}, \frac{\sigma_{ds}}{\lambda}, \frac{\sigma_{fu}^n}{\lambda}, f, f', \bar{\delta}\right) \tag{22}$$

where $\bar{\sigma}_c = 4\sigma_c/(V_f E_f)$ and $\bar{\delta} = (1 + \eta)\hat{\delta}$. Eq. (22) shows that the normalized bridging stress is fully determined by six fundamental micromechanical parameters. The original FRPM is recovered if σ_{ds}/λ and f' are set to zero. λ is an interface friction related parameter defined under (1).

PREDICTING IMPORTANT COMPOSITE CHARACTERISTICS

Experimental Program and Focused Characteristics

The proposed theory enables us to predict properties critical for PSH composite design. The peak composite bridging stress σ_{peak} and corresponding COD δ_{peak}, which form peak point in σ_c-δ relation, are focused as the important composite properties for composite design. This is because that PSH composites can be realized when the complementary energy of σ_c-δ curve exceeds the fracture toughness of the matrix (Marshall and Cox 1988; Li 1993), and this complementary energy seems to have a strong correlation with the peak properties. Hence, these important properties, σ_{peak} and δ_{peak}, are compared with experimental data, and this comparison is aimed at supporting the validity of the proposed theory.

TABLE 1. Matrix Mix Proportion

Cement (1)	Sand (2)	Water (3)	Super plasticizer (4)	Viscous agent (5)
1.0	0.40	0.45	0.02	0.002

For this comparison purpose, uniaxial tensile tests were conducted with a PVA fiber composite, whose matrix mix proportion is summarized in Table 1. The composite was designed to show multiple cracking and resulting PSH behavior. The composite design procedure is described in a companion paper (Kanda and Li 1998c, in press). A 2% volume fraction of PVA fiber having 40 μm diameter and 12 mm length was used. The fiber mechanical properties can be found in Table 2. This fiber system is found to have chemical-dominant fiber-matrix interface properties, $\tau_i \approx 2$ and $\tau_s \approx 30$ MPa (Kanda and Li 1998a). In contrast, polyethylene (PE) fiber has practically no chemical bond. Furthermore, the PVA fiber composite will involve fiber rupture due to the very high bond strengths combined with relatively low fiber strength ($\sigma_{fu}^n \approx 800$ MPa), as shown in Table 2. Two tensile test specimens were tested, whose geometry is shown in Fig. 4. The specimens have an 80-mm-long center portion, which was used as the gauge length for tensile strain measurement employing two LVDTs. The other loading condition was described in greater detail elsewhere (Akihama et al. 1982). In addition, COD was closely examined for all the generated multiple cracks after failure using optical microscope ($\times$ 400 magnification). The mean value is referred to as the mean postmortem COD δ_{peak}^{test}. Postmortem COD was confirmed to represent CODs at the end of multiple cracking sequence (''ultimate state,'' hereafter), where tension softening initiates (Kanda and Li 1998b). This is because crack closure was found insignificant even after complete unloading (less than 10%). The detailed procedure of this examination was explained in Kanda and Li (1998b).

This peak point should correspond to composite peak stress σ_{peak}^{test} and the mean postmortem COD δ_{peak}^{test} observed in uniaxial tensile tests. For PSH composites with multiple cracks, it was indicated that the σ_c-δ relations vary from crack to crack due to statistical variability of micromechanics parameters for fiber, fiber-matrix interface, and matrix (Kanda and Li 1998b). Nevertheless, the theoretical prediction of peak stress, σ_{peak}, appears to correspond to peak stress observation in test, σ_{peak}^{test} (Kanda 1998). The δ_{peak} was also demonstrated to correspond to δ_{peak}^{test}, although the postmortem COD was found to have a wide distribution range (Kanda and Li 1998b).

TABLE 2. Constitutive Parameters for Composite

Constituent (1)	Micromechanical parameter (2)	40 μm-PVA composite (3)	14 μm-PVA composite (4)	Polyethylene composite[b] (5)
Fiber	Fiber length L_f (mm)	12	6	12.7
	Fiber diameter d_f (mm)	0.040	0.014	0.038
	Fiber elastic modulus E_f (GPa)	21.8	60	117
	Nominal fiber strength σ_{fu}^n (MPa)	806[a]	1,666[a]	2,400
	Fiber volume fraction V_f (%)	2	1.5	2
Matrix	Matrix elastic modulus E_m (GPa)	23	23	23
Fiber/matrix interface	Friction bond strength τ_i (MPa)	2.21[a]	4.35[a]	0.7
	Chemical bond strength τ_s (MPa)	31.3[a]	33.6[a]	—
	Snubbing coefficient f	0.5[c]	0.5[c]	0.8
	Fiber strength reduction factor f'	0.3[c]	0.3[a]	—

[a]After Kanda and Li (1998a).
[b]After Li et al. (1995).
[c]Assumed.

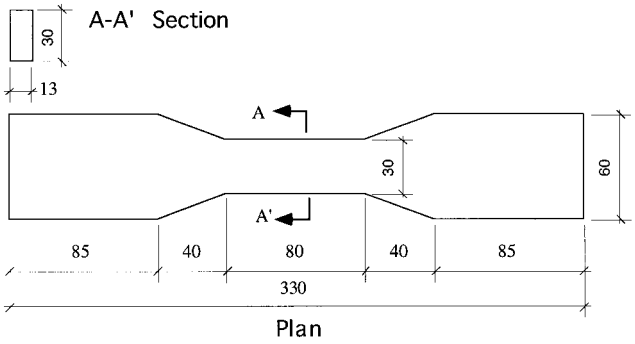

FIG. 4. Tensile Specimen Geometry

Experimental Result in Comparison with Theory

The adopted composite showed PSH behavior with multiple cracking. The measured tensile stress-strain relation (Fig. 5) shows remarkable strain capacity over 1%. The averaged σ_{peak}^{test} is 3.09 MPa. The high strain capacity is attributed to multiple cracking, which is represented by fine cracks perpendicular to the loading axis shown in Fig. 6. Microscope investigation was conducted to measure the postmortem COD (Fig. 7), the distribution of which is summarized in Fig. 8. The postmortem COD varies from less than 10 μm to over 70 μm, while many cracks have COD less than 40 μm. A mean value of 22 μm was determined for δ_{peak}^{test}. Similar postmortem COD variation was reported for a PE fiber composite (Kanda and Li 1998b).

Theoretical σ_c-δ relation was calculated using (21) and the composite's micromechanics parameters tabulated in column 3 of Table 2. No data are currently available for this composite's fiber strength reduction factor f' and snubbing coefficient f among the parameters in Table 2. As in this table, $f' = 0.3$

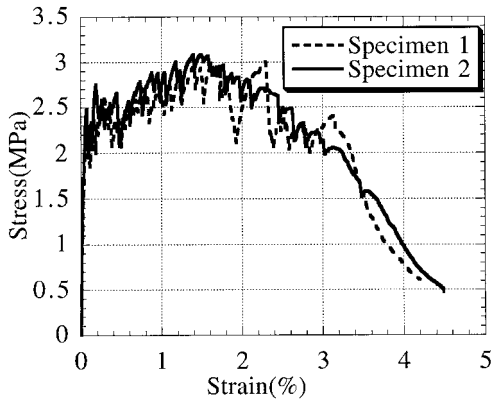

FIG. 5. Tensile Stress-Strain Relation in Test

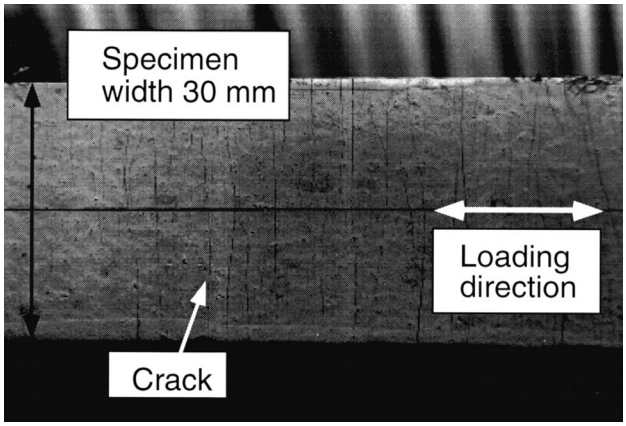

FIG. 6. Multiple Cracking Developed in Specimen

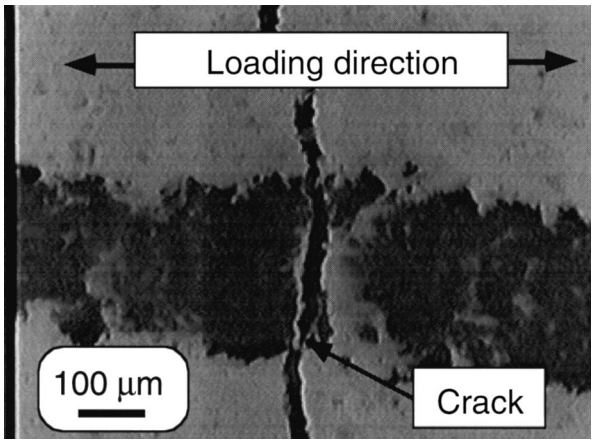

FIG. 7. Crack Investigation under Microscope (×400 Magnification)

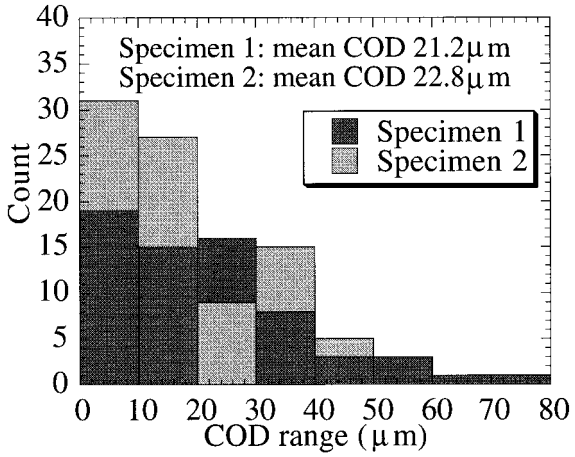

FIG. 8. Distribution of Postmortem Crack Opening Displacement

was adopted using data for a similar PVA fiber with a different diameter (14 μm) (Kanda and Li 1998a). Furthermore, $f = 0.5$ was assumed as the lower bound of reported values for polymeric fiber with cement matrix, e.g., 0.5–0.8 for PE fiber (e.g., Li et al. 1995), 1.0 for nylon fiber, 0.7 for polypropylene fiber (Li et al. 1990), and 0.6 for Aramid fiber (Maalej et al. 1995). Only Aramid fiber is considered to have a notable chemical bond due to its hydrophilic surface chemistry, among these fiber types (Kanda and Li 1998a). The reason for adopting a low bound value for PVA fiber is that that snubbing effect is essentially to increase apparent frictional bond strength, rather than chemical bond strength. Hence the snubbing effect may become less significant for stronger chemical bond–dominant interfaces like PVA fibers.

The resulting theoretical prediction for the peak bridging performance was found to almost agree with test data. The employed parameters led to $L_c = 3.31$ mm via (9), and therefore $L_f = 12$ mm $> 2L_c$ is satisfied for the investigated composite. Hence (21) can be adopted instead of (20), and the theoretical σ_c-δ curve was then calculated as indicated in Fig. 9. This theoretical prediction has a peak at $\delta = 0.0148$ mm and $\sigma_c = 3.51$ MPa, which are reasonably consistent with the test results of $\delta_{peak}^{test} = 0.022$ mm and $\sigma_{peak}^{test} = 3.09$ MPa, considering significant statistical variation in individual cracks' postmortem COD as demonstrated in Fig. 8. As a result, this comparison provides limited support for the proposed theory in evaluating important characteristics of high-performance hydrophilic-fiber-reinforced composites.

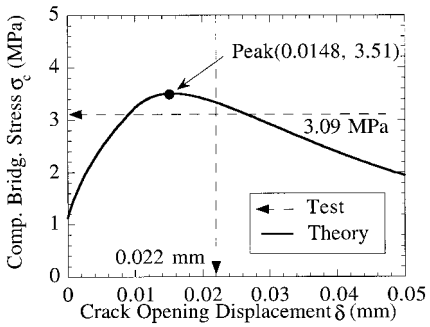

FIG. 9. Comparison of σ_c-δ Relation between Theory and Test Result

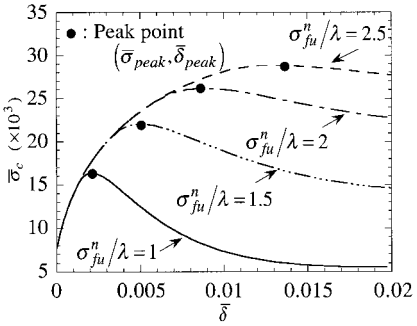

FIG. 11. Effect of Nominal Fiber Strength on Normalized Stress-COD Relation ($E_f/\lambda = 50$; $\sigma_{ds}/\lambda = 0.125$; $f = 0.5$; $f' = 0.3$)

PARAMETRIC STUDY

The presented $\bar{\sigma}_c - \bar{\delta}$ relation is governed by the micromechanical parameters shown in (22). The influence of the newly introduced nondimensional quantities σ_{ds}/λ, σ^n_{fu}/λ, and f' is illustrated through parametric studies, which employ realistic values of the micromechanical parameters. These parameters for the primary composite system used in this study (E_f/λ = 50, σ_{ds}/λ = 0.125, σ^n_{fu}/λ = 2, f = 0.5, and f' = 0.3) were determined by adopting the intermediate properties between those of three composite systems, the 40 μm-PVA fiber composite in this study, a 14 μm-PVA fiber composite (Kanda and Li 1998a,c), and a polyethylene fiber composite (Li et al. 1995) summarized in Table 2, since these three composites may represent extremes. The 40 μm-PVA fiber system has very high bond strengths but low fiber aspect ratio L_f/d_f (≈ 300) and fiber strength σ^n_{fu} as aforementioned. The 14 μm-PVA fiber system has extremely high bond strengths ($\tau_i \approx 4$ and $\tau_s \approx 30$ MPa) and high L_f/d_f (≈ 430) but medium σ^n_{fu} (≈ 1,650 MPa). The PE fiber system has very high σ^n_{fu} (≈ 2,400 MPa), but low bond strengths ($\tau_i \approx 0.5$ and $\tau_s \leq 0.5$ MPa) and L_f/d_f (≈ 330).

The effects of the first micromechanical parameter, σ_{ds}/λ, are depicted in Fig. 10. The σ_{ds}/λ can be regarded as a measure of the chemical to frictional bond ratio (for a given fiber aspect ratio). In this figure, the peak point of $\bar{\sigma}_c$-$\bar{\delta}$ curve was expressed as $(\bar{\sigma}_{peak}, \bar{\delta}_{peak})$. This figure illustrates that peak stress $\bar{\sigma}_{peak}$ increases but COD $\bar{\delta}_{peak}$ at the peak stress decreases with increase of chemical bond strength, which shows solid circles for the peak points $(\bar{\sigma}_{peak}, \bar{\delta}_{peak})$. Furthermore, composite stress $\bar{\sigma}_c$ ($\bar{\delta}$ = 0) increases with chemical bond strength, and its nonzero value is a result of neglecting elastic deformation of the matrix foundation in (23). This assumption is valid because the matrix deformation is negligibly small, as explained in Appendix I. These effects lead to a significant reduction in the complementary energy of the σ_c-δ curves as can be geometrically deduced from Fig. 10. Because the complementary energy is one of the most important properties for PSH composite design, this issue is discussed in more detail in the

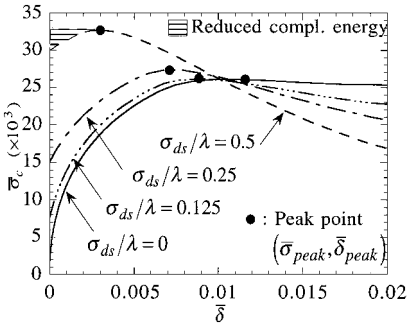

FIG. 10. Effect of Chemical Bond Strength on Normalized Stress-COD Relation ($E_f/\lambda = 50$; $\sigma^n_{fu}/\lambda = 2$; $f = 0.5$; $f' = 0.3$)

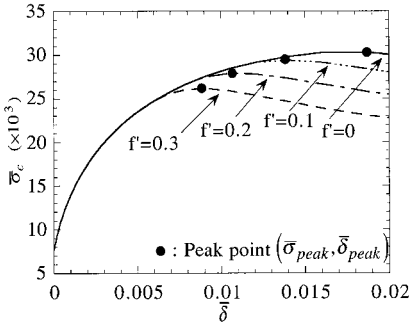

FIG. 12. Effect of Fiber Strength Reduction Factor on Normalized Stress-COD Relation ($E_f/\lambda = 50$; $\sigma_{ds}/\lambda = 0.125$; $\sigma^n_{fu}/\lambda = 2$; $f = 0.5$)

companion paper (Kanda and Li 1998c). The effects of the second micromechanical parameter, σ^n_{fu}/λ, are illustrated in Fig. 11, which shows that both $\bar{\sigma}_{peak}$ and $\bar{\delta}_{peak}$ increase with σ^n_{fu}. The opposite trend to Fig. 11 is observed in Fig. 12, which illustrates the effects of the third parameter f'. Fig. 12 shows that both $\bar{\sigma}_{peak}$ and $\bar{\delta}_{peak}$ decrease with increase of f', which negatively affects the bridging performance of composites.

These parametric studies revealed that the magnitude of the newly introduced parameters remarkably affect the bridging performance prediction. This implies that neglecting these parameters is not acceptable, as it leads to inaccurate evaluation of composite performance. Furthermore, the ultimate goal of this study—to design PSH composite with high-performance hydrophilic fiber—may be achieved by tailoring the magnitude of these parameters.

CONCLUSIONS

This study is aimed at developing a comprehensive bridging law (relation between crack-bridging stress due to fiber, σ_c, and crack opening displacement δ), focusing on cementitious composites containing high-strength polymeric fibers with a hydrophilic surface nature, such as PVA fibers. The new theory accounts for two new features: (1) chemical dominant bond property and (2) fiber strength reduction and rupture in composite, and extends a preexisting crack bridging law to cover a broader range of fiber types. As a result, three new micromechanical parameters—chemical bond strength τ_s, nominal fiber strength σ^n_{fu}, and fiber strength reduction factor f'—are introduced into the σ_c-δ relation.

The new bridging law as found capable of predicting a composite's important crack bridging characteristics, i.e., the peak bridging stress σ_{peak} and corresponding COD δ_{peak}. This was confirmed in comparison with uniaxial tensile test data employing a PVA fiber composite. The σ_{peak} and δ_{peak} were experimentally obtained from recorded stress-strain relation and postmortem COD measurements. Consistency in theory prediction and experimental observation for σ_{peak} and δ_{peak} pro-

vides confidence in using the proposed bridging model, which appears quite useful in pseudo strain hardening (PSH) composite design.

Furthermore, parametric studies of the resulting bridging law revealed that the newly accounted fiber and interface parameters significantly affect bridging performance, which should be reflected in PSH composite design procedures. The completion of this design goal contributes to additional confidence in the validity of the bridging model described in this article. The detailed investigation for this goal is described in a companion paper (Kanda and Li 1998c).

APPENDIX I. SINGLE-FIBER STRESS-COD RELATION ON DEBONDING PROCESS

Chemical-type interface can be accounted for in the relationship between single-fiber bridging stress at exit point from the matrix, σ_d, and crack-opening displacement, δ, based on the model by Li and Leung (1992). Through experiments, Kanda and Li (1998a) have confirmed this model as capable of representing interface properties of hydrophilic fibers. The σ_d-δ relationship was expressed as

$$\frac{\delta}{d_f} = \left(\frac{\sigma_d}{E_f}\right)\left(\frac{2L_d}{d_f}\right) - \frac{\tau_i E_c \left(\frac{2L_d}{d_f}\right)^2}{E_f V_m E_m} \tag{23}$$

where L_d = debonding length; E_c = elastic modulus of composite; V_m = volume fraction of matrix; E_m = elastic modulus of matrix; τ_i = frictional bond strength; d_f = fiber diameter; and E_f = elastic modulus of fiber. Furthermore, fiber stress was expressed as a function of debonding length, by assuming that deponding proceeds as τ_s is overcome and chemical bond is replaced with friction represented τ_i

$$\sigma_d = \frac{\left[2\left(\frac{2L_d}{d_f}\right)\tau_i \cosh Z + 2\left(\frac{\tau_s}{\rho}\right)\sinh Z\right]}{(1-\alpha)\cosh Z + \alpha} \tag{24}$$

where $Z = 2\rho(L_f - L_d)/d_f$, $\alpha = V_f E_f/E_c$, $\rho^2 = 2G_c E_c/[V_m E_m E_f \log(2R^*/d_f)]$. R^* = effective radius of matrix cylinder containing fiber; τ_s = chemical bond strength; and G_c = shear modulus of composite. Budiansky et al. (1986) derived as $\log(2R^*/d_f) = -[2\log V_f + V_m(3 - V_f)]/(4V_m^2)$ in the above. Assuming $Z >> 0$ may be appropriate except for the final stage of debonding, resulting in

$$\tanh Z \cong 1 \tag{25}$$

Eq. (24) can be further simplified by considering $\alpha << 1$ and employing (25)

$$\sigma_d = \frac{\left[2\left(\frac{2L_d}{d_f}\right)\tau_i + 2\left(\frac{\tau_s}{\rho}\right)\right]}{(1-\alpha)} \tag{26}$$

Eliminating L_d with (23) and (26) leads to

$$\sigma_d = \{\sigma_{di}^2 + \sigma_{ds}^2\}^{1/2} \tag{27}$$

where $\sigma_{di} \equiv [4(1+\eta)E_f\tau_i(\delta/d_f)]^{1/2}$ and $\sigma_{ds} \equiv [2(1+\eta)(\tau_s/\rho)$. The first term of the right-hand side of (27) represents the contribution of friction bond, and the second term represents that of chemical bond, to resisting load on the fiber.

The $L_{d\text{peak}}$ is defined here as the debonding length at which fiber stress reaches maximum. Beyond $L_{d\text{peak}}$, load drops unstably if the fiber has strong chemical interface bond. This mechanism was examined in detail by Leung and Li (1991). The assumption represented by (25), on which the derivation of (26) is based, holds as long as the $L_{d\text{peak}}$ is close to the embedment length l. This assumption is not valid if a fiber-matrix system has much higher chemical bond strength than frictional bond strength. However, even for the PVA fiber with extremely strong chemical bond strength, as shown in Table 1, calculation with (26) showed $L_{d\text{peak}}/l = 0.9$ with peak fiber stress overestimated by 5% relative to that of the exact expression (24). Therefore, this assumption is considered valid in the practical range of fiber-matrix systems. The following, a normalized form of (27), is expressed as (28)′, and normalized single fiber stress σ_d/τ_i is shown for different bond strength ratio τ_s/τ_i in Fig. 13:

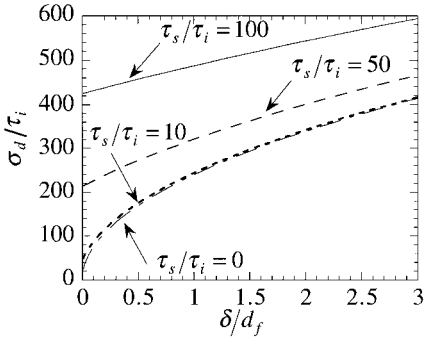

FIG. 13. Influence of Chemical Bond Strength on Single-Fiber Stress

$$\frac{\sigma_d}{\tau_i} = \left\{4(1+\eta)\left(\frac{E_f}{\tau_i}\right)\left(\frac{\delta}{d_f}\right) + \frac{4(1+\eta)^2}{\rho^2}\left(\frac{\tau_s}{\tau_i}\right)^2\right\}^{1/2} \tag{28}$$

Fig. 13 illustrates the stress increasing effect of chemical bond strength. Furthermore, it shows $\sigma_d/\tau_i > 0$ at $\delta = 0$ when $\tau_s/\tau_i > 0$. This is resulted by neglecting elastic deformation of matrix foundation in the derivation of (23), whose contribution is usually much smaller than that of the two terms in (23) (Li and Leung 1992). Hence only the negligible deformation δ exists prior to overcoming the chemical bond.

By suitable normalization, (27) is finally expressed in the form of (3).

APPENDIX II. SINGLE-FIBER STRESS-COD RELATION ON PULL-OUT PROCESS

Eq. (26) gives the single-fiber maximum stress $\sigma_{\max}$ when debonding length L_d is equal to embedment length l, which corresponds to a full debonding state along the fiber embedment length. The $\sigma_{\max}$ might be approximated as follows by assuming $1 - \alpha \approx 1$ (appropriate for low $V_f << 1$ with polymeric fibers which have relatively lower elastic modulus) in (26)

$$\sigma_{\max} = \sigma_{ds} + \left(\frac{4}{\pi d_f^2}\right)(\pi d_f \tau_i l) = \sigma_{ds} + 4\tau_i\left(\frac{l}{d_f}\right) \tag{29}$$

δ_0, the displacement at $\sigma_{\max}$, can be derived by equating (29) to (27)

$$\hat{\delta}_0 = \hat{\delta}_i^*\left[\hat{l}^2 + 2\left(\frac{\sigma_{ds}}{\lambda}\right)\hat{l}\right] \tag{30}$$

The $\hat{\delta}_{0i}$ in (2) corresponds to $\hat{\delta}_0$ when $\sigma_{ds} = 0$ is assumed. Substituting $\hat{\delta}_{0i}$ in (2) by using $\hat{\delta}_0$ in (30), (4) for σ_p is derived.

APPENDIX III. CURRENT FIBER-RUPTURE ANGLE

During debonding process, single-fiber bridging stress σ_b is expressed as a function of inclining angle ϕ and COD δ as shown in (5). Hence, COD δ_u, at which σ_b attains fiber-rupture strength σ_{fu}, depends on ϕ as follows [using (6)]:

$$\hat{\delta}_u(\phi) = \hat{\delta}_{ci}[e^{-2(f+f')\phi} - \xi^2] \tag{31}$$

where $\hat{\delta}_{ci} = \hat{\delta}_i^* \hat{L}_{ci}^2$. Then current fiber-rupture angle ϕ_c, below which fiber rupture has not yet occurred at certain COD δ, is obtained by equating δ to δ_u in (31)

$$\phi_c(\hat{\delta}) = -\frac{1}{2(f+f')} \ln\left[\left(\frac{\hat{\delta}}{\hat{\delta}_i^*}\right)\frac{1}{\hat{L}_{ci}^2} + \xi^2\right] \tag{32}$$

The ϕ_c takes constant $\pi/2$ before fiber rupture starts at $\delta = \delta_u(\phi = \pi/2)$, and decreases with increase of COD δ as shown by (32). Then, it is eventually reduced to ϕ_b at $\delta = \delta_{ue}$ (δ_{ue} denotes the COD when the debonding process of each fiber is terminated). All population of fibers proceeds to the pull-out process beyond δ_{ue}, which is calculated with the following formula:

$$\hat{\delta}_{ue} = \begin{cases} \hat{\delta}^* = \hat{\delta}_0(l=1) = \hat{\delta}_i^*[1 + 2\beta] & \text{for } L_r < L_f < 2L_c \\ \hat{\delta}_c = \hat{\delta}_u(\phi = 0) = \hat{\delta}_{ci}[1 - \xi^2] & \text{for } 2L_c < L_{fc} \end{cases} \tag{33}$$

Finally, ϕ_c is expressed in the form of (12) by employing the above discussion.

APPENDIX IV. BRIDGING STRESS-COD RELATION FOR COMPOSITES

The debonding stage represented by (18) is divided into two substages at the COD when fiber rupture is initiated ($\delta_u(\phi = \pi/2)$). Before fiber rupture starts, the integrals in (18) are evaluated by using (3), (4), (7), (10), and (12). Considering $\phi_c = \pi/2$ prior to rupture initiation, this calculation results in the next formula for any fiber length

$$\sigma_c = \sigma_{0i} C_A G\left(\frac{\pi}{2}, f\right) \quad \text{for } 0 \le \delta \le \delta_u\left(\phi = \frac{\pi}{2}\right) \tag{34}$$

where $C_A = \{2/3\hat{\delta}_i^*\gamma^{3/2} - 2\hat{\delta}_i^*\gamma^{1/2}\beta^2 + 4/3\hat{\delta}_i^*\beta^3 - \gamma + 2\gamma^{1/2} + \beta^2 - 2\hat{\delta}\gamma^{1/2} + 2\hat{\delta}\beta - 2/3\hat{\delta}_i^*\hat{\delta}^3 + \hat{\delta}^2 - 2\hat{\delta}_i^*\hat{\delta}^2\beta\}$. After fiber rupture initiates, (18) gives the following results:

For $L_r \le L_f \le 2L_c$:

$$\sigma_c = \sigma_{0i}\left\{\begin{array}{l} C_A G(\phi_c, f) \\ + C_{B1}A(\phi_c, -2f - 3f') + C_{B2}A(\phi_c, -f - 2f') \\ + C_{B3}A(\phi_c, -f') + C_{B4}A(\phi_c, f) \end{array}\right\} \quad \text{for } \delta_u\left(\phi = \frac{\pi}{2}\right) \le \delta \le \delta^* \tag{35}$$

For $L_f > 2L_c$:

$$\sigma_c = \sigma_{0i}\left\{\begin{array}{l} C_A G(\phi_c, f) \\ + C_{B1}A(\phi_c, -2f - 3f') + C_{B2}A(\phi_c, -f - 2f') \\ + C_{B3}A(\phi_c, -f') + C_{B4}A(\phi_c, f) \end{array}\right\} \quad \text{for } \delta_u\left(\phi = \frac{\pi}{2}\right) \le \delta \le \delta_c \tag{36}$$

where $C_{B1} = 2/3\hat{\delta}_i^*\hat{L}_{ci}^3$; $C_{B2} = (1 + 2\beta\hat{\delta}_i^*)\hat{L}_{ci}^2 - 2\hat{\delta}_i^*\hat{L}_{ci}^3\xi$; $C_{B3} = 2\hat{\delta}_i^*\hat{L}_{ci}^3\xi^2 - 2(1 + 2\beta\delta_i^*)\hat{L}_{ci}^2\xi - 2\hat{\delta}\hat{L}_{ci}$; and $C_{B4} = (1 + 2\beta\hat{\delta}_i^*)\hat{L}_{ci}^2\xi^2 - 2/3\hat{\delta}_i^*\hat{L}_{ci}^3\xi^3 + 2\hat{\delta}\hat{L}_{ci}\xi - 2/3\hat{\delta}_i^*\hat{\delta}^3 + (1 - 2\beta\hat{\delta}_i^*)\hat{\delta}^2$.

Similar to the debonding stage, the pull-out stage is divided into two substages at the COD when complete fiber pull-out initiates ($= L_r/2$). For the first substage, the integral in (19) is calculated in the same manner as (18) by utilizing (3), (4), (7), (10), and (14). Considering $\phi_a = \pi/2$ for $\delta < L_r/2$, this calculation yields the next formula

For $L_r \le L_f \le 2L_c$:

$$\sigma_c = \sigma_{0i}\left\{\begin{array}{l} C_C G(\phi_b, f) \\ + C_{B1}A(\phi_b, -2f - 3f') + C_{B2}A(\phi_b, -f - 2f') \\ + C_{B3}A(\phi_b, -f') + C_{B4}A(\phi_b, f) \end{array}\right\} \quad \text{for } \delta^* \le \delta \le \frac{L_r}{2} \tag{37}$$

For $L_f > 2L_c$:

$$\sigma_c = \sigma_{0i}\left\{C_{B1}G\left(\frac{\pi}{2}, -2f - 3f'\right) + C_{B2}G\left(\frac{\pi}{2}, -f - 2f'\right) + C_{B3}G\left(\frac{\pi}{2}, -f'\right) + C_{B4}G\left(\frac{\pi}{2}, f\right)\right\} \quad \text{for } \delta_c \le \delta \le \frac{L_r}{2} \tag{38}$$

where $C_C = 2/3\hat{\delta}_i^* + (1 + 2\beta\hat{\delta}_i^*) - 2\hat{\delta} - 2/3\hat{\delta}_i^*\delta^3 + (1 - 2\beta\hat{\delta}_i^*)\hat{\delta}^2$. The second substage starts when the COD reaches $L_r/2$, and is represented by the following formula derived from (19):

For $L_r \le L_f \le 2L_c$:

$$\sigma_c = \sigma_{0i}\left\{\begin{array}{l} C_C G(\phi_b, f) + C_{B1}B(\phi_b, \phi_a, -2f - 3f') \\ + C_{B2}B(\phi_b, \phi_a, -f - 2f') + C_{B3}B(\phi_b, \phi_a, -f') \\ + C_{B4}B(\phi_b, \phi_a, f) \end{array}\right\} \quad \text{for } \frac{L_r}{2} \le \delta \le \frac{L_f}{2} \tag{39}$$

For $L_f > 2L_c$:

$$\sigma_c = \sigma_{0i}\{C_{B1}G(\phi_a, -2f - 3f') + C_{B2}G(\phi_a, -f - 2f') + C_{B3}G(\phi_a, -f') + C_{B4}G(\phi_a, f)\} \quad \text{for } \frac{L_r}{2} \le \delta \le L_c \tag{40}$$

$\hat{\delta}_i^* << 1$ and $\hat{\delta} << 1$ can be assumed for debonding stage. $\hat{\delta}_i^* << 1$ is also true for pull-out stage. Hence, (34)–(40) are simplified as in (20) and (21) by neglecting higher-order terms.

ACKNOWLEDGMENTS

This manuscript was completed when V. C. Li was a Visiting Professor at the University of Tokyo, Japan. Part of this research was supported by a grant (CMS-EQ-9601262) from the National Science Foundation to the University of Michigan at Ann Arbor. Special thanks are due to Mr. J. Hikasa in Kuraray Co., Ltd. (Osaka, Japan) for helpful discussion and material supplied. T. Kanda acknowledges valuable advice from Dr. H. C. Wu, Dr. Z. Lin (at University of Michigan), and Dr. M. Maalej.

APPENDIX V. REFERENCES

Akihama, S., Suenaga, T., and Banno, T. (1982). ''Experimental study of carbon fiber reinforced cement composites—'CFRC' (Part II).'' *Kajima Annu. Tech. Rep.*, Kajima Corporation, 30, 123–128 (in Japanese).

Akihama, S., Suenaga, T., Nakagawa, H., and Suzuki, K. (1985). ''Experimental study of vinylon fiber reinforced cement composites—'VFRC' (Part I).'' *Kajima Annu. Tech. Rep.*, Kajima Corporation, 33, 123–128 (in Japanese).

Bao, G., and Suo, Z. (1993). ''Crack bridging models for fiber reinforced composites with slip-dependent interfaces.'' *J. Mech. Phys. Solids*, 41(9), 1425–1444.

Bao, G., and Song, Z. (1992). ''Remarks on crack-bridging concept.'' *Micromechanical modeling of quasi-brittle materials behavior*, V. C. Li, ed., American Society of Mechanical Engineers, New York, 355–366.

Betterman, L. R., Ouyang, C., and Shah, S. P. (1995). ''Fiber-matrix interaction in microfiber-reinforced mortar.'' *Advanced Cement Based Mat.*, 3(2), 53–61.

Budiansky, B., Hutchinson, J. W., and Evans, A. G. (1986). ''Matrix fracture in fiber-reinforced ceramics.'' *J. Mech. Phys. Solids*, 34(2), 167–189.

Gao, Y. C., Mai, Y. W., and Cotterell, B. (1988). ''Fracture of fiber reinforced materials.'' *J. Appl. Math. Phys.*, 39, 550–572.

Goplaratnam, V. S., and Shah, S. P. (1985). ''Tensile fracture of steel fiber reinforced concrete.'' *J. Engrg. Mech.*, ASCE, 113(4), 635–653.

Horii, H., and Nanakorn, P. (1993). ''Fracture mechanics based design on SFRC tunnel lining.'' *Size effect in concrete structures*, H. Mihashi, H. Okamura, and Z. P. Bazant, eds., E&FN Spon, London, 429–440.

Hutchinson, J. W., and Jensen, H. M. (1990). ''Models of fiber debonding and pullout in brittle composites with friction.'' *Mech. of Mat.*, 9, 139–163.

Kanda, T. (1998). ''Design of engineered cementitious composites for ductile seismic resistant elements,'' PhD thesis, University of Michigan, Ann Arbor, Mich.

Kanda, T., and Li, V. C. (1998a). ''Interface property and apparent

strength of a high strength hydrophilic fiber in cement matrix.'' *J. Mat. in Civ. Engrg.*, ASCE, 10(1), 5–13.
Kanda, T., and Li, V. C. (1998b). ''Multiple cracking sequence and saturation in fiber reinforced cementitious composites.'' *Concrete Res. and Tech.*, 9(2), 1–15.
Kanda, T., and Li, V. C. (1998c). ''A new micromechanics design theory for pseudo strain hardening cementitious composite.'' *J. Engrg. Mech.*, ASCE, in press.
Kelly, A., and Tyson, W. R. (1965). ''Tensile properties of fiber-reinforced metals: Copper/tungsten and copper/molybdenum.'' *J. Mech. Phys. Solids*, 13, 329–350.
Leung, C. K. Y., and Li, V. C. (1991). ''New strength-based model for the debonding of discontinuous fibers in an elastic matrix.'' *J. Mat. Sci.*, 26(11), 5996–6010.
Li, V. C. (1993). ''From micromechanics to structural engineering—the design of cementitious composites for civil engineering applications.'' *J. Struct. Mech. Earthquake Engrg.*, 10(2), 37–48.
Li, V. C., and Leung, K. Y. (1992). ''Steady-state and multiple cracking of short random fiber composites.'' *J. Engrg. Mech.*, ASCE, 118(11), 2246–2263.
Li, V. C., Mishra, D. K., and Wu, H. C. (1995). ''Matrix design for pseudo-strain hardening fiber reinforced cementitious composites.'' *Mat. and Struct.*, 28(183), 586–595.
Li, V. C., Wang, Y., and Backer, S. (1990). ''Effect of inclining angle, bundling, and surface treatment on synthetic fiber pull-out from a cement matrix.'' *Composites*, 21(2), 132–140.
Maalej, M., Li, V. C., and Hashida, T. (1995). ''Effect of fiber rupture on tensile properties of short fiber composites.'' *J. Engrg. Mech.*, ASCE, 121(8), 903–913.
Marshall, D. B., and Cox, B. N. (1987). ''Tensile fracture of brittle matrix composites: Influence of fiber strength.'' *Acta Metallurgica*, 35(11), 2607–2619.
Marshall, D. B., and Cox, B. N. (1988). ''A j-integral method for calculating steady-state matrix cracking stresses in composites.'' *Mech. of Mat.*, 7, 127–133.
Marshall, D. B., Cox, B. N., and Evans, A. G. (1985). ''The mechanics of matrix cracking in brittle-matrix fiber composites.'' *Acta Metallurgica*, 33(11), 2013–2021.
Naaman, A. E., and Reinhardt, H. W. (1995). ''High performance fiber reinforced cement composites.'' *RILEM Proc. 31*, E&FN Spon, London.
Outwater, J. O., and Murphy, M. C. (1970). ''Fracture energy of unidirectional laminates.'' *Modern Plastics*, 47(9), 160–169.
Shao, Y., Li, Z., and Shah, S. P. (1993). ''Matrix cracking and interface debonding in fiber-reinforced cement-matrix composites.'' *Advanced Cement-Based Mat.*, 1(1), 55–66.
Stang, H., Li, V. C., and Krenchel, H. (1995). ''Design and structural applications of stress-crack width relations in fiber reinforced concrete.'' *J. of Mat. and Struct.*, 28, 210–219.
Takaku, A., and Arridge, R. G. C. (1973). ''The effect of interfacial radial and shear stress on fiber pull-out in composite materials.'' *J. Phys. D: Appl. Phys.*, 6, 2038–2047.